Planetary and Space Science 216 (2022) 105477

Contents lists available at ScienceDirect

Planetary and Space Science

journal homepage: www.elsevier.com/locate/pss

The astrometric results of observations of fast-moving NEAs during close approach to the Earth

Anton Pomazan [a,b,c,*], Zheng-Hong Tang [a,c], Nadiia Maigurova [d], Yong Yu [a,c], Kai Tang [a], Yin-Dun Mao [a], Ye-Zhi Song [a]

[a] Shanghai Astronomical Observatory, Chinese Academy of Sciences, 80 Nandan Rd., Shanghai, 200030, China
[b] University of Chinese Academy of Sciences, Beijing, 100049, China
[c] School of Astronomy and Space Science, University of Chinese Academy of Sciences, Beijing, 100049, China
[d] Research Institute "Mykolaiv Astronomical Observatory", Mykolaiv, 54030, Ukraine

ARTICLE INFO

Keywords:
methods: observational
Techniques: miscellaneous
Astrometry
Minor planets
Asteroids: general
Celestial mechanics

ABSTRACT

Current investigation is devoted to ongoing follow-up observations of fast-moving near-Earth asteroids (NEAs) carried out with Rotating-drift-scan CCD technique on small-aperture telescopes in China and Ukraine. The observations were obtained during closest approach (CA) to the Earth in order to get more observational points and extend observational arc. It is especially important for newly discovered NEAs when high-precision astrometry is required to determine and improve the orbital elements making them recoverable in next apparitions. The latest astrometric results of NEAs observations, particularly for newly discovered ones, are presented and analyzed in order to refine their orbits and estimate possible recovery in next CA. The comparative analysis of astrometric positions and orbital elements were done regarding to International Astronomical Union Minor Planet Center database and JPL's HORIZONS ephemerides system. The residual differences (O – C) often show high values for newly discovered NEAs during observation date which explained by lack of available observations for reliable calculations of ephemerid positions. The data for such NEAs is presented and orbital calculations are done.

1. Introduction

Near-Earth asteroids (NEAs), and potentially hazardous asteroids (PHAs) as special part of them, being the most accessible group of objects of natural origin are important for studying the Solar system in general and near-Earth space in particular. Except purely scientific interests like dynamical evolution and migration of small Solar System bodies, distribution of water and materials and transportation it to the Earth region, there are applied investigations of future possible collision of such objects with the Earth and for-profit exploration including near-future spacecraft mining missions (Xie et al., 2021). Furthermore, even if the statistical risk is quite low, there is a nonzero probability of a collision of PHA with the Earth, which can lead to catastrophic consequences both at the local level and for mankind in general (Perna et al., 2013).

Recent size-frequency distribution and completion of NEAs population assessments (Harris and Chodas, 2021; Heinze et al., 2021) combining with current discovery state of new NEAs (the statistics could be seen at the Center for Near-Earth Object Studies (CNEOS) website,[1] NASA JPL) assume vast number of undiscovered small-size objects. Considering the data described in the most recent investigation (Harris and Chodas, 2021) the population of discovered NEAs with $H \leq 22$ mag (larger than 140 m) is 9582 objects, which represent around 44% of population model estimation. At the same time, due to their small size which results in faint apparent brightness, such NEAs are discovered in a short interval of their close approach (CA) to the Earth, when their apparent magnitude tend to be brighter for a given size, which facilitates the discovery of smaller asteroids by surveys. However, the investigation presented in Veres et al. (2012) shows that apparent rate of motion for objects at small CA distances (within 10 lunar distances) generally exceeds 25 $''$ min^{-1} (10 deg day^{-1}), making the observations of such objects challenging. Insufficient number of observations for newly discovered NEAs or low accuracy of the obtained positions leads to inaccurate determination of the orbits and to increasing the uncertainty in its position. Such uncertainty might grow dramatically over the years resulting in impossible to carry out new observations during following apparitions and cause lose asteroids completely. Poorly observed NEAs and especially PHAs with insufficiently precise orbits are priority targets for observations

* Corresponding author. Shanghai Astronomical Observatory, Chinese Academy of Sciences, 80 Nandan Rd., Shanghai, 200030, China.
E-mail address: antpomaz@shao.ac.cn (A. Pomazan).

[1] Center for Near-Earth Object Studies, https://cneos.jpl.nasa.gov/stats/totals.html.

https://doi.org/10.1016/j.pss.2022.105477
Received 17 December 2021; Received in revised form 28 March 2022; Accepted 2 April 2022
Available online 6 April 2022

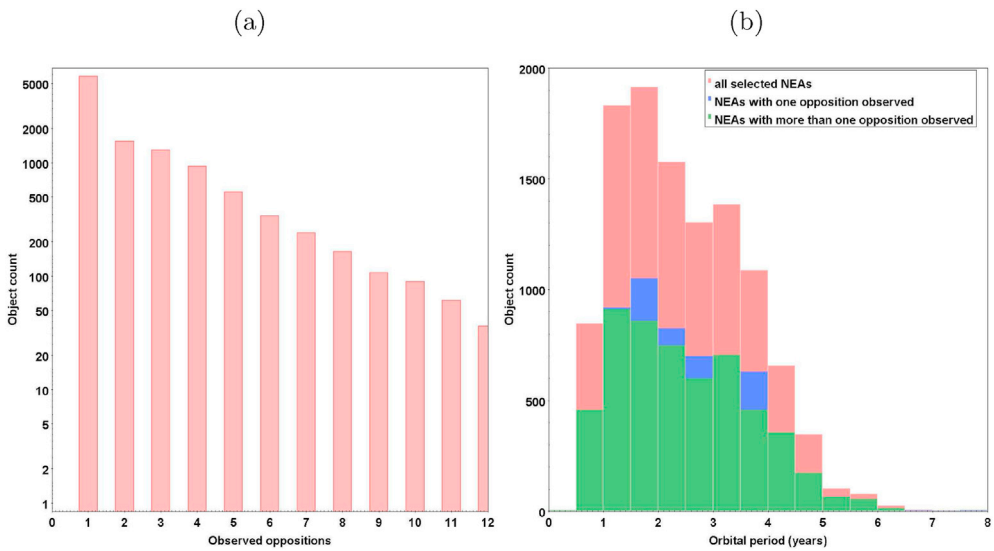

Fig. 1. The histograms of distributions of NEAs discovered during 2000–2015 regarding to: a) observed oppositions (left panel), the number of objects is plotted on a log scale; b) orbital period (right panel).

during next oppositions in order to improve their orbits and to prevent object losses (Vaduvescu et al., 2018). Bowell et al. (1997) noted, it is required to obtain sufficient amount of positions at discovery apparition with geometrically increasing time intervals. It is important in order to calculate near future positions with enough accuracy. As well as that fixed number could be assigned to NEA (which supposed it's orbit is well-determined) after two or three apparitions with successful observations during several nights. Such observations made during a second apparition other than the discovery one are defined as recovery (Boattini and Forti, 2000).

Rapid follow-up observations are necessary for newly discovered NEAs and especially PHAs before their sky uncertainties grow too large and apparent magnitudes become too faint to detect. Accurate positions obtained during discovery apparition allow to recover these objects in next apparitions. In the same time, during unsuccessful or unavailable follow-up observational program, around 11% of new discoveries of NEAs remain unconfirmed and could be lost. The high rate of apparent motion is considered as one of significant contributing factors (Veres et al., 2018; Heinze et al., 2021).

The article represents the results of ongoing follow-up observations of fast-moving near-Earth asteroids (NEAs) carried out with Rotating-drift-scan CCD (RDS CCD) technique (Tang et al., 2014). The observations were conducted on the telescope of the Lishan Observing Station (National Time Service Center of Chinese Academy of Sciences, NTSC of CAS, China; hereinafter: Lishan telescope) and the KT-50 telescope (RI Mykolaiv Astronomical Observatory, Ukraine; hereinafter: KT-50 telescope). The significant part of observations was obtained around time moment of minimum distance to the Earth during considered CA for newly discovered NEAs when apparent rate of motion substantially exceeds diurnal motion. The used RDS CCD observational technique allows to avoid trailing loss for fast-moving objects (FMO) and yields precise astrometry comparable to best ground-based optical observations of NEAs independent to rate of apparent motion.

In this paper, Section 2 analyzes possibilities for extending observed orbital arc during discovery apparition and recovery observations of NEAs in next oppositions; Section 3 shows the instrument information and observational statistics; Section 4 describes the methods of astrometric reduction used to measure the positions of NEAs and Section 5 shows the obtained astrometric results.

2. Recovery possibilities of NEAs

The modern theoretical studies (Roa et al., 2020) show the probabilities of asteroid recovery observations in the future, as well as the current practical results for existed observations (Boattini and Forti, 2000; Vaduvescu et al., 2018) depending on the telescope class. According to Roa et al. (2020) in the next 50 years among all known NEAs with $H \leq 22$ mag the 74% of population are recoverable, 16% are potentially recoverable, and only 10% are not recoverable. Considering only PHA population, the majority of objects are recoverable (83%) with remaining 10% and 7% as potentially recoverable and not recoverable, respectively.

At the present, however, analysis of statistical information about collected NEAs observations presented in the International Astronomical Union Minor Planet Center database[2] (hereinafter: MPC) performed by observed oppositions as input parameter shows that more than 50% of considered NEAs (5755 objects) have been observed only at one opposition (Fig. 1a). In this case, only NEAs with discovery date between 2000 and 2015 were chosen for analysis. The choice of this time span is explained by attempt, on one side, to select only CCD observations (which a priori have higher positional accuracy in comparison with earlier photographic observations), on the other side, to exclude objects, as possible, with orbital periods which don't allow to obtain observations at the next oppositions (to avoid some bias in presented distribution). Such big number of NEAs observed only at one opposition might be explained by their long orbital periods. But as distribution on Fig. 1b shows, the most of considered NEAs have orbital periods less than 4 years with peak placed around 2 years. Therefore, it should be possible to observe these objects during up to 7 oppositions on considered time span. As it can be seen, distribution of orbital periods doesn't have much difference between objects with one observed opposition and multiple ones.

Such small number of recovered NEAs can be explained by next reasons, among others: a) insufficiently precise orbits, resulting in big displacement between real and predicted position at next opposition so these objects are out of field of view (FOV) of a telescope; b) due to the mutual placement geometry of Sun-Target-Observer, the object has an apparent magnitude available for optical observations only with large telescopes; c) lack of coordinated observational companies. The specialized algorithm for efficiently planning and executing NEO follow-up observations (recovery) was developed (Boattini et al., 2007) and established online service with Priority list.[3] Such service increases

[2] International Astronomical Union Minor Planet Center, https://minorplanetcenter.net/iau/MPCORB.html.

[3] Priority List of European Space Agency NEO Coordination Centre, https://neo.ssa.esa.int/priority-list.

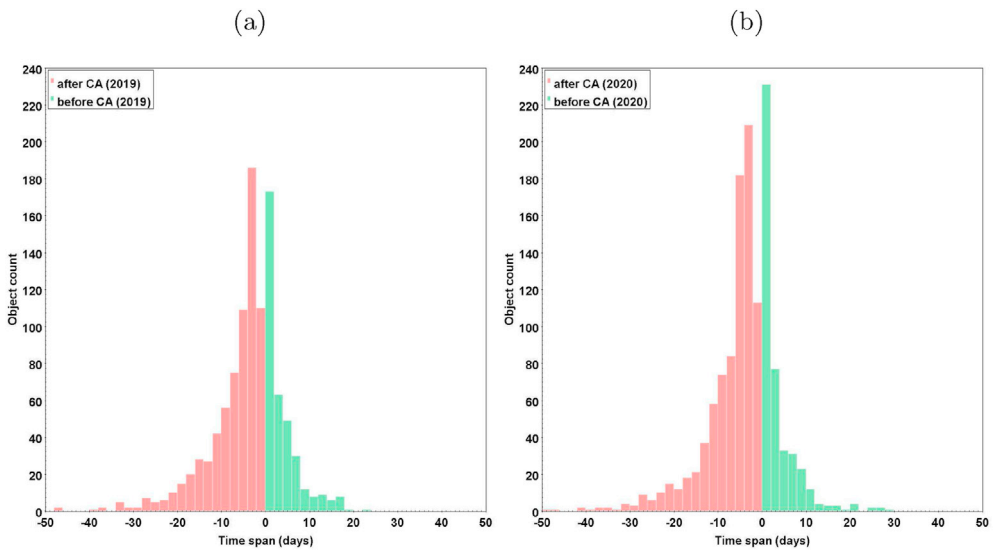

Fig. 2. Distribution of newly discovered NEAs according their existed positions with respect to the time moment of minimum distance to the Erath in a) 2019 and b) 2020. The histograms are plotted with 2 days bin. The distributions are plotted over time difference (in days) between specified time moment and: first position in observed orbital arc (in other words, all observations are taken after CA, red color); last position in observed orbital arc (all positions are before CA, green color).

Table 1
Observational statistics of newly discovered NEAs regarding to time moment of the minimum distance to the Earth.

Year	2019		2020	
Total amount	1741		2245	
before CA	360	21%	429	19%
inside	648	37%	923	41%
after CA	733	42%	893	40%

probability of these bodies can be recovered at other apparitions. As well as the MPC provides their own list with poorly observed currently-observable NEAs required new astrometric positions.[4] The first listed reason could be solved by finding and linking archived observations or obtaining additional observations during the discovery apparition to increase number of precise observations and extend observed orbital arc. As an example, the analysis of the data for newly discovered NEAs in 2019–2020 available at MPC database linked with the time moments of minimum distance to the Earth taken from CNEOS system was performed. The selected NEAs were divided into 3 groups defined by their observations with respect to CA time moment. The distributions presented on Fig. 2 show the data only for 2 considered groups: 1) all existing positions were obtained after the time moment of minimum distance to the Earth during specified CA (red left part of histograms); 2) all existing positions were obtained before the specified time moment of CA to the Earth (green right part of histograms). A difference between the time moment of minimum distance to the Earth and the *first* obtained position is calculated for objects from the first defined group, while a difference between the specified time moment and the *last* position in existing dataset for NEA is calculated for objects in the second group. Hence, the distributions show how many objects and which time differences do they have between their observed orbital arcs and the time moments of minimum distance to the Earth. The third group when the time moment of minimum distance at CA is inside of the observed orbital arc was not considered in the current analysis but general observational statistics could be seen on Table 1. It could be seen that: 1) around 40% (42% in 2019 and 40% in 2020) of the total number of considered objects were discovered after their CA time moment and shows potential danger

[4] IAU MPC One-Opposition Unnumbered Objects, https://minorplanetcenter.net/iau/NEO/LastObsNEO.html.

Table 2
Main specifications of optical imaging systems.

Telescope	Focal length (mm)	CCD FOV (′)	Scale ($''\ px^{-1}$)	FWHM (′)
Lishan telescope	3445	36.7 × 36.7	0.72	2.3
KT-50 telescope	3000	42.5 × 42.5	0.83	2.5

of untimely detection of such NEAs; 2) there is a significant part (around 10% for each considered year of observations) of objects for which an increase of observed orbital arc is possible by observations taken during the day of minimum distance to the Earth and, as a consequence, some increase in their brightness. If considering only one day of the time difference between last taken observation and time moment of CA the exact numbers are 105 objects in 2019 and 149 objects in 2020. In the same time, it is worth remember, the increasing in apparent rate of motion and significant orbit inclination of such NEAs can impose additional restrictions on the exposure time. It should also be taken into account that in such distribution, the most NEAs have the time moment of minimum distance to the Earth during CA inside observed orbital arc. The results shown by these distributions confirm the results derived in Maigurova et al. (2018).

3. Astrometric observations

As it mentioned above the purpose of the project is obtaining high precision astrometric positions of NEAs during the CA to the Earth in order to get more observational data for refining and improving orbit determination. The analyzed here arrays of NEAs CCD observations were obtained at the Lishan telescope (code O85) and the KT-50 telescope (code 089) during 2020–2021. Both telescopes equipped by Alta U9000 CCD camera with array 3056 × 3056 pixels of size 12 μm. The CCD camera allows to work in TDI mode, thus RDS CCD technique is implemented on both telescopes to perform observations of FMO. The short specifications of instruments are shown in Table 2. More detailed information of RDS CCD technique and telescope technical characteristics could be found in Pomazan et al. (2021).

During considered observational period the 1215 astrometric positions of 76 NEAs were obtained on LiShan telescope (code O85) and 2898 positions for 74 NEAs - on KT-50 telescope (code 089). The observational statistics of obtained positions averaged by the year in case of both

telescopes is presented in Table 3. The total number of obtained positions and observed objects during specified year are presented in the columns N1, N2, correspondingly; as well as columns n1, n2 contain the same but only for newly discovered objects in considered year. The Table 3 column (O – C) represents differences calculated for obtained "O" astrometric positions regarding to ephemerid "C" ones computed by JPL's HORIZONS ephemeris system,[5] NASA JPL.

Among observed NEAs on considered telescopes there are 19 newly discovered objects for Lishan telescope with 231 obtained positions and 7 objects with 58 obtained positions on KT-50 telescope. The information about observed newly discovered NEAs taken from MPC database and own analysis of observations listed in Table 4. The columns N1 and N2 contain amount of observations obtained at considered telescope and general amount of existed observations respectively. The column "**App. motion**" shows the apparent rate of motion at the time moment of minimum distance to the Earth during current CA ("**max**.", calculated with respect to Geocenter) and mean apparent rate of motion during obtained observations ("**mean**", with respect to observational site). As can be seen, these NEAs have not defined well orbits (just three objects have uncertainty parameter equal or less than 2 which means well defined orbit) due to small amount of existed observations and observed orbital arc. Part of these objects were observed at date of CA when apparent rate of motion reaches the maximum value and for two of them (K21C00O, K21C06A) the observations obtained at Lishan observational station are the last ones in observational arc. In Table 4 columns "**Obs.**" in "**UTC date**" and "**mean**" in "**App. motion**" represent the date and apparent rate of motion, respectively, for obtained observations closest to CA date. The average rate of motion for obtained array of positions for newly discovered NEAs is 60.8 $''\,\mathrm{min}^{-1}$ (29.3 deg day^{-1}) with the highest value equal 386.4 $''\,\mathrm{min}^{-1}$ (154.6 deg day^{-1}). It worth noting, some NEAs (K20C01X, K20G02D, K20Q06V, K20W05U, K21C02K, K21E05C, and K21M01K) which considered as discovered in 2020–2021 have the first observations obtained much earlier. But only with new observations these objects were confirmed and their orbits were determined good enough to assign provisional designations for them.

3.1. Observations of NEOCP objects

The observations of objects from NEO Confirmation Page[6] (NEOCP, Marsden and Williams, 1998) are performed among regular already known NEAs. These objects are newly-discovered and mostly are fast-moving ones with not yet assigned provisional designations from the MPC on current date. Alert observations are required to reliable determination of their orbits. It should be noted, available list contains all newly discovered objects which could not be linked with known space objects. Erroneous artifacts and objects of artificial origin are also present there.

The Scout[7] and NEOScan[8] provided by CNEOS and NEODyS systems, respectively, are ephemerid services additionally to MPC one. All mentioned services use the same initial astrometric data but different computational algorithms which result in different calculated ephemerides. In some cases, the differences of these ephemerides significantly exceed FOV of considered here telescopes. During preparation to observations of NEOCP objects the ephemerides computed by Scout and NEOScan services were used to create an observational program on specified date. The resulting observational statistics of these objects on KT-50 telescope presented in Table 5. In case of successful detection of the target object, the obtained topocentric positions are immediately sent to the MPC database.

Table 3
Observational statistics of NEAs for Lishan and KT-50 telescopes.

Year	IAU MPC	N1	N2	Current year		(O – C) $\pm\,\sigma('')$	
	code			n1	n2	RA	Dec
2020	O85	464	35	33	3	-0.01 ± 0.13	-0.03 ± 0.16
2020	089	1435	35	60	7	0.00 ± 0.18	-0.02 ± 0.22
2021*	O85	751	55	312	19	0.00 ± 0.15	-0.02 ± 0.15
2021*	089	1494	38	58	7	0.05 ± 0.20	0.07 ± 0.24

* Data regarding on December 2021.

As could be seen from Table 5, the percentage of successful confirmations in case of KT-50 telescope is small. Most of performed observations were unsuccessful (see the column "**Notes**" of the Table 5) due to too faint apparent brightness or inaccurate predicted ephemerid caused small amount of initial positions. As a rule, an object that has not been confirmed for a time period of more than 1 day is lost. Some objects after additional observations were confirmed as artificial satellites or space debris.

4. Astrometric reduction software

The observations analyzed in current research were obtained using RDS CCD technique which allows to obtain pointed images of target objects with high apparent rate of motion. The implemented technique assumes to obtain at least three CCD frames during one observational set while telescope stays fixed at certain position in order to place the CCD frame with an image of the object between CCD frames for reference stars. In following astrometric processing, it is necessary to take such separated observations into account and reduce position of the object to coordinate system of reference stars.

The astrometric reduction of CCD frames with stars is standard and made by well-known *Astrometrica* software[9] with *Gaia* Data Release 2 (*Gaia* DR2) star catalogue (Gaia Collaboration et al., 2016, 2018) as reference system. The software measures rectangular coordinates (x, y) of field stars in CCD frame system, computes equatorial coordinates for them and related plate constants in the Turner's method equations[10] for these CCD frames. The next step supposes to interpolate calculated plate constants to the middle exposure time moment of CCD frame with target object. Due to diurnal motion of celestial sphere the equatorial coordinates of the points at the same positions in a FOV of a telescope with respect to optical center are changed with time. Should also remember that technical realization of imaging system is strictly saying nonperfect (e.g., the CCD matrix is not exactly parallel to focal plane and a center point of CCD matrix does not coincide with optical axis of the telescope). It results in some changes of parameters described by the plate constants (i.e., scales in both directions, angles between axes of standard and measured coordinates, etc.). Such changes, namely changes of some plate constants, could not be approximated using simple linear interpolation. More straightforward is to use horizontal coordinates instead. Since telescope is fixed at certain position during one set of observations (which takes up to 3 min), the horizontal coordinates of CCD frame centers are constant and the relationship between horizontal standard coordinate system and rectangular coordinate system of CCD matrix are unchanged during considered time interval as well. Minor changes are

[5] JPL HORIZONS online Solar system data and ephemeris computation service, https://ssd.jpl.nasa.gov/horizons/app.html#/

[6] The IAU MPC The NEO Confirmation Page, https://minorplanetcenter.net/iau/NEO/toconfirm_tabular.html.

[7] Scout: NEOCP Hazard Assessment, https://cneos.jpl.nasa.gov/scout/#/

[8] NEODyS: NEOScan, https://newton.spacedys.com/neodys/NEOScan/index.html.

[9] Astrometrica software, http://www.astrometrica.at.

[10] The method was proposed by H. H. Turner in 1893 and determines the relationship between the idealized coordinates (ξ, η) and the measured rectangular coordinates (x, y) of celestial bodies by reduction equations involving power series.

Table 4
Newly discovered NEAs observed at Lishan telescope (O85) and KT-50 telescope (089).

NEA	IAUMPC	UTC Date			N1	N2	Obs-ed.orb.arc	Uncert.param.	rms	App. Motion, ($''min^{-1}$)	
	code	Disc.	Obs.	CA			(days)		($''$)	max.	mean
K20G02D	O85	2020-04-10	2020-04-23	2020-04-17	12	429	201	2	0.39	16.3	8.9
K20M03X	O85	2020-06-28	2020-07-27	2020-07-29	11	153	32	4	0.34	29.2	25.2
K20N01K	O85	2020-07-13	2020-07-27	2020-07-31	10	122	19	7	0.49	46.3	16.9
K20C01X	O85	2020-02-05	2021-02-16	2021-02-18	16	171	1107	0	0.88	54.5	42.3
K20W05U*	O85	2020-11-29	2021-01-13	2021-01-13	66	277	3855	1	0.34	32.8	32.8
K21C00O*	O85	2021-02-05	2021-02-11	2021-02-11	15	86	6	6	0.62	395.5	386.6
K21C02K	O85	2021-02-07	2021-02-11	2021-02-07	29	193	204	3	0.63	34.2	18.9
K21C06A*	O85	2021-02-10	2021-02-13	2021-02-13	22	66	3	4	0.71	505.2	336.4
K21D01W	O85	2021-02-16	2021-03-03	2021-03-04	14	269	27	3	0.68	117.5	82.2
K21D01X	O85	2021-02-20	2021-03-03	2021-02-23	6	228	40	5	0.71	19.9	9.1
K21E05C	O85	2021-03-14	2021-05-26	2021-05-21	17	229	3685	0	0.72	5.3	4.8
K21F00H	O85	2021-03-18	2021-03-22	2021-03-23	10	92	5	7	0.58	631.1	25.6
K21F01K	O85	2021-03-20	2021-03-23	2021-03-24	15	49	4	7	0.71	284.1	53.4
K21J01X	O85	2021-05-04	2021-06-04	2021-06-07	12	173	42	5	0.69	15.2	14.2
K21J02H	O85	2021-05-05	2021-09-09	2021-08-09	9	419	188	4	0.50	7.5	2.3
K21K00C	O85	2021-05-16	2021-05-19	2021-05-21	5	109	25	4	0.66	32.3	26.3
K21Q03B	O85	2021-08-31	2021-09-09	2021-09-03	7	291	59	4	0.63	122.8	2.2
K21R02G	O85	2021-09-06	2021-09-07	2021-09-06	5	186	4	5	0.77	33.9	31.5
K21U01W	O85	2021-10-27	2021-10-29	2021-10-30	14	146	4	6	0.55	447.1	32.6
K21U09M*	O85	2021-10-26	2021-11-13	2021-11-13	34	200	19	6	0.61	79.4	78.6
K21V02R	O85	2021-11-06	2021-11-09	2021-11-10	9	68	4	6	0.65	177.8	80.8
K21V03V	O85	2021-11-07	2021-11-08	2021-11-06	7	142	7	8	0.52	106.2	25.5
K20N01K	089	2020-07-13	2020-07-29	2020-07-31	3	108	19	7	0.49	46.4	25.1
K20P04T	089	2020-08-13	2020-09-06	2020-09-08	4	38	25	6	0.23	82.1	40.8
K20Q06V	089	2020-08-28.	2020-08-30	2020-08-28	19	167	3257	0	0.64	67.8	31.6
K20R00C	089	2020-09-03	2020-09-07	2020-09-06	10	275	21	5	0.35	41.6	35.9
K20R00J*	089	2020-09-05	2020-09-08	2020-09-08	7	120	5	4	0.44	91.1	88.9
K20R06Z	089	2020-09-15	2020-09-18	2020-09-17	9	92	3	5	0.74	315.9	229.8
K20S00W	089	2020-09-18	2020-09-23	2020-09-24	8	229	6	5	0.33	3414.6	32.4
K21E05C	089	2021-03-14	2021-05-26	2021-05-21	11	229	3685	0	0.72	5.3	4.8
K21J01G	089	2021-05-03	2021-05-25	2021-05-26	10	178	24	5	0.62	134.2	97.9
K21K00C	089	2021-05-16	2021-05-19	2021-05-21	7	109	25	4	0.66	32.3	27.4
K21M01E	089	2021-06-21	2021-06-27	2021-07-27	8	116	14	5	0.78	58.6	56.5
K21M01K	089	2021-06-23	2021-06-28	2021-07-27	3	309	1896	1	0.62	17.9	17.5
K21N04M*	089	2021-07-11	2021-07-12	2021-07-12	10	70	6	6	0.84	102.4	102.2
K21R14J	089	2021-09-12	2021-09-13	2021-09-11	9	86	5	6	0.59	64.7	51.9

* Observations obtained at date of CA.

caused by different sets of reference points (the set of horizontal coordinates will not be the same due to both different reference stars and the same refence stars but different places).

A set of Turner's equations with plate constants in horizontal standard coordinate system can be solved by combining measured rectangular coordinates of reference stars on the corner CCD frames together:

$$\begin{cases} \xi_{1i} = f(x_{1i}, y_{1i}, a, b, c, \ldots) \\ \eta_{1i} = g(x_{1i}, y_{1i}, d, e, f, \ldots) \\ \xi_{2j} = f(x_{2j}, y_{2j}, a, b, c, \ldots) \\ \eta_{2j} = g(x_{2j}, y_{2j}, d, e, f, \ldots) \end{cases} \quad i = 1, m; j = 1, n \tag{1}$$

where (ξ_{1i}, η_{1i}), (ξ_{2j}, η_{2j}) and (x_{1i}, y_{1i}), (x_{2j}, y_{2j}) are the horizontal standard and measured rectangular coordinates of the reference stars on the corner CCD frames, respectively; m and n are the numbers of the reference stars on these two frames; and $(a, b, c, \ldots)$ and $(d, e, f, \ldots)$ represent the plate constants according to order of equations in Turner's method. The 4th order polynomial function in Turner's equations was used to eliminate errors which occur due to differential refraction, decentering error, tilting error, CCD camera distortion and etc. As shown in Yu et al. (2018), combination of reference stars from corner CCD-frames from one observational set to solve the equations of plate model parameters gives increasing of standard deviations of the (O – C) residuals than those calculated by single CCD-frame. For that reason, combination method was used only in case of small number of reference stars when it was impossible to apply the 4th order of Turner's equations.

Since *Astrometrica* software results only in equatorial coordinates of identified stars the additional software was developed in ShAO to transform such results to horizontal coordinate system as well as recalculate plate constants for new coordinates. The software written in Python programming language[11] (version 3.x) using specific libraries (modules) for scientific mathematical and astronomical calculations such as: NumPy (Harris et al., 2020); SciPy (Virtanen et al. 2020); Astropy (Astropy Collaboration et al., 2013); PALpy (Jenness and Berry, 2013).

The horizontal coordinates of identified stars were calculated based on two SLALIB routines (SLA_MAP and SLA_AOP) adopted for Python by PALpy module. These routines implement the concept of calculations to transform: 1) mean places of stars to geocentric apparent places; 2) geocentric apparent places to observed ones. The backward transformation is carried out according to the reverse concept using SLALIB routines (SLA_OAP and SLA_AMP) for its realization as well. The standardized values of average atmospheric conditions are used as input parameters, among others, to considered functions.

The new standard coordinates computed from horizontal ones were used in order to link the rectangular coordinates of identified stars in the system of CCD frame to spherical coordinates. The computations of the equation systems with plate model constants for each coordinate were performed by non-linear least squares method implemented in *scipy.optimize* module by several iterations. Each time, the new center coordinates calculated based on the new plate constants were compared with the previous calculations and changes equal to or less than $0.001''$ were taken as criteria to stop the iterations.

Calculated plate constants, horizontal coordinates of CCD frame center and determined rectangular coordinates of object's image center

[11] Python programming language, https://www.python.org/.

Table 5
Observed NEOCP objects on KT-50 telescope.

NEOCPname	Assigned prov.design.	Obs.time span.	Available/obtainedpositions	Obs. date	Notes
A10yYKv	K21N04M	2021-07-11 – 2021-07-17	64/10	2021-07-12	MPS 1432900 MPEC 2021-O23
C28NMZ1	K21R14J	2021-09-12 – 2021-09-17	86/9	2021-09-13	MPS 1462254 MPEC 2021-R309
A10BBf9	–	–	–	2021-09-30	was not confirmed (Oct. 5.55 UT)
A10ZxKL	–	–	–	2021-08-14	was not confirmed (Aug. 18.05 UT)
P11iZpm	–	–	–	2021-08-23	was not confirmed (Aug. 31.21 UT)
A10zk8o	K21O01G	2021-07-30 – 2021-08-17	48/0	2021-07-30	Too faint
A10zu84	K21P00J	2021-08-03 – 2021-08-16	144/0	2021-08-03	Too faint
A10BNNG	–	–	–	2021-10-05	was suspected artificial (Oct. 6.93 UT)
C2AVDW1	–	–	–	2021-10-05	was suspected artificial (Oct. 5.56 UT)

Table 6
Astrometric statistics of selected newly discovered NEAs with apparent rate of motion more than 30 $''$ min^{-1}.

NEA	IAUMPC	UTC	num	(O – C) ± $\sigma('')$			
	code	(UTC)		RA	Dec	along-track	cross-track
K20C01X	O85	2021-02-16	16	0.03 ± 0.14	−0.19 ± 0.17	−0.13 ± 0.15	−0.15 ± 0.15
K20W05U	O85	2021-01-11	21	−0.02 ± 0.07	−0.01 ± 0.08	0.01 ± 0.09	−0.02 ± 0.06
K20W05U	O85	2021-01-12	10	0.05 ± 0.13	−0.09 ± 0.13	0.10 ± 0.12	0.02 ± 0.12
K20W05U	O85	2021-01-13	7	−0.07 ± 0.10	0.14 ± 0.11	−0.16 ± 0.12	−0.03 ± 0.07
K20W05U	O85	2021-01-17	18	−0.04 ± 0.07	0.01 ± 0.12	−0.03 ± 0.10	−0.02 ± 0.09
K20W05U	O85	2021-01-18	10	−0.07 ± 0.17	0.03 ± 0.17	−0.07 ± 0.20	−0.03 ± 0.11
K21C00O	O85	2021-02-10	7	0.06 ± 0.14	0.06 ± 0.11	0.08 ± 0.15	0.04 ± 0.07
K21C00O	O85	2021-02-11	8	0.63 ± 0.16	0.50 ± 0.16	0.79 ± 0.16	0.15 ± 0.14
K21C06A	O85	2021-02-13	22	−2.03 ± 0.25	−0.05 ± 0.18	−2.01 ± 0.25	0.31 ± 0.17
K21D01W	O85	2021-03-03	14	−0.18 ± 0.10	−0.17 ± 0.14	−0.24 ± 0.14	0.08 ± 0.09
K21F00H	O85	2021-03-22	10	−0.01 ± 0.13	−0.14 ± 0.17	0.07 ± 0.17	−0.13 ± 0.10
K21F01K	O85	2021-03-23	15	0.24 ± 0.28	−0.24 ± 0.29	0.34 ± 0.15	−0.02 ± 0.35
K21R02G	O85	2021-09-07	5	0.21 ± 0.39	−0.05 ± 0.26	−0.01 ± 0.20	−0.22 ± 0.37
K21U01W	O85	2021-10-29	14	0.08 ± 0.18	0.15 ± 0.36	0.07 ± 0.17	0.15 ± 0.35
K21U09M	O85	2021-11-09	6	0.07 ± 0.20	0.03 ± 0.29	0.01 ± 0.25	0.07 ± 0.20
K21U09M	O85	2021-11-10	7	0.11 ± 0.23	−0.07 ± 0.09	0.12 ± 0.17	0.04 ± 0.15
K21U09M	O85	2021-11-12	8	0.12 ± 0.07	−0.04 ± 0.13	0.13 ± 0.10	0.06 ± 0.09
K21U09M	O85	2021-11-13	13	0.21 ± 0.07	0.04 ± 0.14	0.19 ± 0.07	0.09 ± 0.14
K21V02R	O85	2021-11-09	9	−0.52 ± 0.23	0.13 ± 0.26	−0.54 ± 0.20	0.04 ± 0.25
K20P04T	089	2020-09-06	4	0.02 ± 0.34	−0.34 ± 0.30	0.02 ± 0.29	−0.34 ± 0.26
K20R00C	089	2020-09-07	10	−0.03 ± 0.13	0.22 ± 0.16	−0.21 ± 0.12	0.07 ± 0.15
K20R00J	089	2020-09-08	7	−0.95 ± 0.32	0.39 ± 0.24	−0.99 ± 0.26	−0.26 ± 0.26
K20R06Z	089	2020-09-18	9	−0.15 ± 0.29	0.01 ± 0.19	−0.07 ± 0.23	−0.13 ± 0.23
K21J01G	089	2021-05-25	10	0.14 ± 0.14	0.23 ± 0.19	0.26 ± 0.16	−0.06 ± 0.15
K21M01E	089	2021-06-27	8	0.18 ± 0.37	0.05 ± 0.37	−0.02 ± 0.34	0.18 ± 0.35
K21N04M	089	2021-07-12	10	−0.07 ± 0.24	0.33 ± 0.35	−0.34 ± 0.34	−0.04 ± 0.21
K21R14J	089	2021-09-13	9	0.08 ± 0.23	0.24 ± 0.24	−0.23 ± 0.23	0.11 ± 0.22

were used to calculate first horizontal coordinates of the object and then transform it to equatorial coordinates. Due to initial equatorial coordinates of reference stars were taken as mean apparent places and transformation both from equatorial coordinates to horizontal ones and vice versa were done using the same parameters and considering observational site, the calculated final equatorial coordinates of the object are topocentric coordinates.

5. Results and precision analysis

Topocentric positions described in current research were compared with JPL's HORIZONS ephemeris system to analyze the accuracy and precision of it. The mean values of the standard deviations σ of (O – C) differences presented in Table 3 can be considered as an estimate of the precision of the obtained positions. These values are around 0.2$''$ in both coordinates for both telescopes and show that obtained positions have good enough precision (Veres et al., 2017).

Moreover, considering newly discovered asteroids only, it is seen that the precision remains at the same level. However, preliminary analysis prior to including these positions in orbit determination shows comparatively big values of (O – C) on date of CA for some of them which most likely are due to insufficient amount of observations for reliable orbit determination. The positional analysis of selected newly discovered NEAs with apparent rate of motion more than 30 $''$ min^{-1} (12 deg day^{-1}) is presented in Table 6. The objects K21C00O, K21C06A, K21U09M, K21V02R and K20R00J show absolute values of (O – C) differences of one coordinate which exceed the values of corresponding standard deviation indicating notable mismatching.

For objects with high apparent rates of motion in plane-of-sky, the timing errors of instrumental system cause significant residuals between observed and ephemerid positions which does not noticeable for slow moving objects. In order to investigate considered telescopes to detect possible timing errors the (O – C) differences expressed in along- and cross-track projections were calculated in addition to usual positional

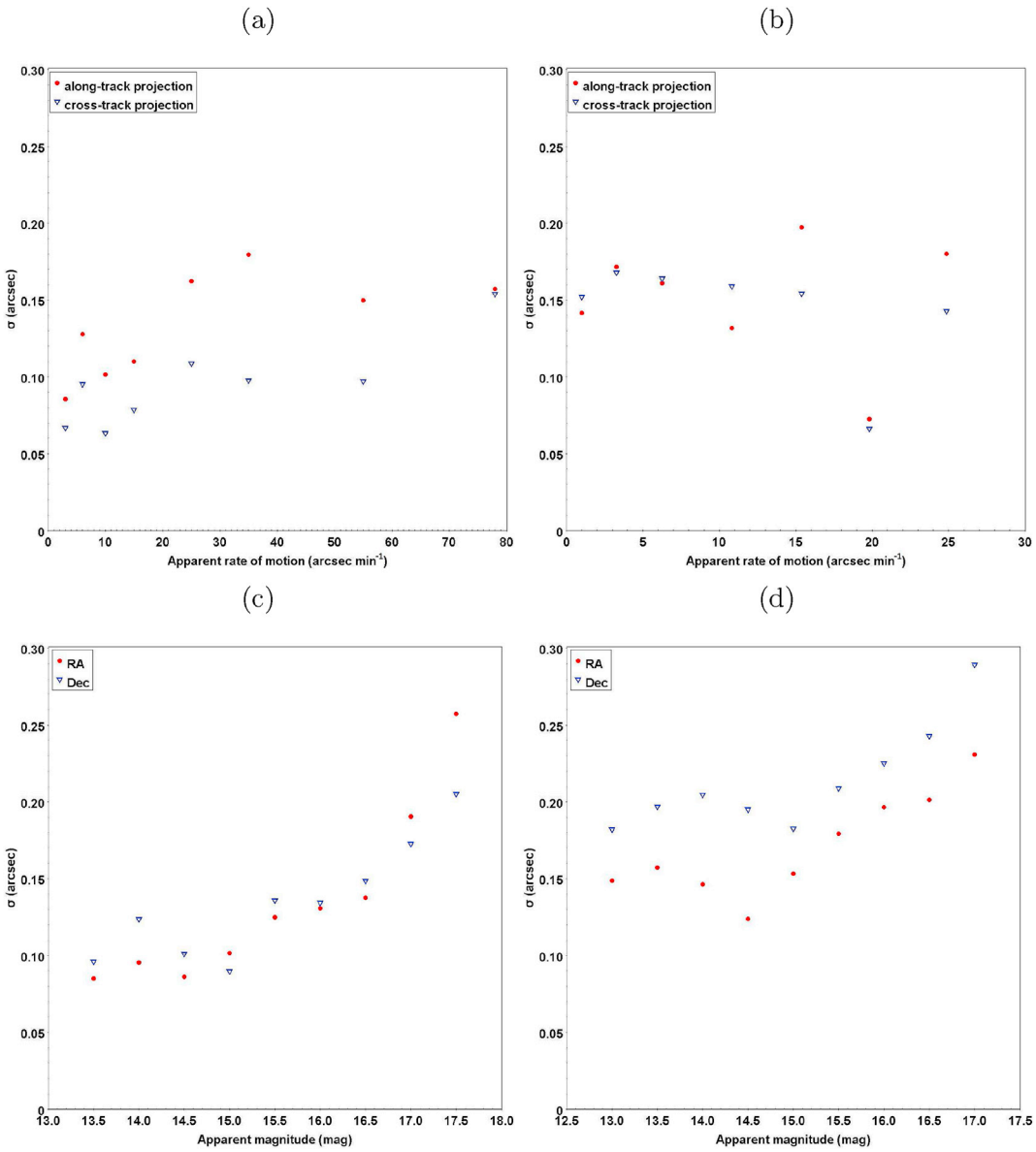

Fig. 3. Standard deviation σ of averaged astrometric residuals (O – C) in along- and cross-track coordinate projections as a function of apparent rate of motion (top panels) and standard deviation σ of (O – C) differences in equatorial coordinates as a function of apparent magnitude (bottom panels) for Lishan telescope (left panels) and KT-50 telescope (right panels). In both cases the mean astrometric residuals of observational series are considered. However, top panels represent dispersion of these mean (O – C) values, while bottom panels show averaged σ values of these mean (O – C) differences. Non-representative data (cases of single and double observational series within considered averaging intervals) were excluded.

offsets in right ascension and declination. These along-/cross-track residuals are computed by rotating equatorial coordinate system to align trajectory and direction of object's apparent motion with one of the coordinate planes (along-track). In this way, along-track residuals will consist of measurement error, ephemerid uncertainty and timing errors, or combination of them, while cross-track ones mainly made up of only measurement errors. Considered RDS CCD technique of observations and processing pipeline were applied for all observations which means the values of introduced errors of centroiding and timing are the same in analyzed array of data. Due to RDS CCD technique allows to obtain both images of reference stars and target objects as pointed sources the centroiding errors are minimal. The along- and cross-track residuals were averaged by 5 $''$ min^{-1} apparent motion intervals (in some cases intervals were reduced or extended if appropriate) and its standard deviation values are plotted on Fig. 3 (top panels) for both telescopes. As could be seen, there are no upward trends in the along-track residuals as a function of the rate of motion which indicates the absence of timing and measurement errors. The range of apparent rate of motion presented on Fig. 3 is limited by 80 $''$ min^{-1} (32 deg day^{-1}) for Lishan telescope and 30 $''$ min^{-1} (12 deg day^{-1}) for KT-50 telescope. Positions for NEAs K21C00O and K21C06A at Lishan telescope and K20R00J, K20R06Z, K21J01G and K21N04M at KT-50 telescope were obtained at higher values of apparent rate of motion with high precision (Table 4 and Table 6).

Fig. 3 (bottom panels) also shows dependencies of positional precision in both coordinates as a function of an apparent magnitude of observed NEAs. The data is averaged over bin 0.5 *mag*. In general, the positions obtained for objects with apparent magnitude more the 17.5 *mag* for Lishan telescope and 17.0 *mag* for KT-50 telescope have much bigger positional errors and such objects are excluded from observations. Presented correlation of standard deviation σ with apparent magnitude is a consequence of dependence of positional precision on signal-to-noise ratio (SNR).

Table 7
The (O – C) differences for NEA 2021 CO (K21C00O).

Date	(O – C), (″)		(O – C), (″)	
	(1)		(2)	
2021.02	RA	Dec	RA	Dec
11.53455	0.90	0.69	0.48	0.41
11.53513	0.46	0.55	0.09	0.22
11.54298	0.47	0.53	0.06	0.19
11.54553	0.68	0.65	0.22	0.39
11.54610	0.55	0.59	0.18	0.26
11.54750	0.80	0.32	0.35	−0.03
11.54808	0.57	0.24	0.20	−0.03
11.55063	0.62	0.39	0.18	0.09
Mean	**0.63**	**0.50**	**0.22**	**0.19**
σ	**0.16**	**0.16**	**0.14**	**0.17**

Table 8
The (O – C) differences for NEA 2021 CA6 (K21C06A).

Date	(O – C), (″)		(O – C), (″)	
	(1)		(2)	
2021.02	RA	Dec	RA	Dec
13.84249	−1.888	−0.206	0.13	−0.049
13.84432	−1.698	0.114	0.327	0.479
13.84614	−2.3	−0.42	−0.348	0.093
13.84796	−1.695	−0.003	0.264	0.257
13.84978	−2.16	−0.051	−0.248	0.138
13.85160	−1.876	0.381	0.241	0.597
13.85343	−2.06	0.017	−0.042	0.311
13.85525	−2.604	0.024	−0.725	0.345
13.85707	−2.039	−0.031	0.098	0.178
13.85889	−2.047	0.052	−0.169	0.358
13.86072	−1.972	−0.091	−0.021	0.163
13.86254	−1.848	0.117	0.149	0.358
13.86436	−1.764	0.095	0.212	0.314
13.86618	−1.697	−0.252	0.232	0.015
13.86801	−1.982	−0.06	0.085	0.134
13.86983	−2.14	−0.103	−0.014	−0.022
13.87165	−1.947	−0.009	−0.08	0.099
13.87348	−2.305	−0.361	−0.234	−0.175
13.87530	−1.893	−0.232	0.131	0.002
13.87870	−1.929	0.103	0.105	0.271
13.88030	−2.362	−0.036	−0.376	0.14
13.88189	−2.412	−0.177	−0.303	0.036
Mean	**−2.03**	**−0.05**	**−0.03**	**0.18**
σ	**0.25**	**0.18**	**0.26**	**0.19**

5.1. Astrometric results at CA date

The astrometric results for two newly discovered NEAs are described below in more details. These cases of fast-moving NEAs observed near the time moment of minimum distance to the Earth are good examples showing the importance of extending observed orbital arc for newly discovered objects and orbital calculations. It also indicates usability and efficiency of RDS CCD technique for targeted observations of FMO.

5.1.1. NEA 2021 CO (K21C00O)

The asteroid was first observed by Catalina Sky Survey on February 5th, 2021 and determined as one of Apollo NEA's group. The minimum distance to the Erath during current CA was 0.00242 AU (or 0.94 lunar distances) at 15:22 on February 11th, 2021 (UTC). However, the MOID is equal to 0.00147 AU which supposes possible approach almost twice closer to the Earth. Up to now there are 105 astrometric positions in MPC database all taken before CA time moment including 15 positions obtained at Lishan telescope on February 10th and 11th. The mean precision is 0.27 ″ in right ascension and 0.23 ″ in declination for other observatories and 0.14 ″ in both coordinates for Lishan telescope. Moreover, the observations at Lishan telescope are last one in existed observed orbital arc and initially had high values of (O – C) differences. Table 7 shows the changes of these residuals in initial calculations (1) and after the positions obtained at Lishan telescope were included to MPC database (2).

It is seen, the absolute values of mean residuals are decreased from 0.63 ″ to 0.22 ″ in RA and 0.50 ″ to 0.19 ″ in declination while precision is kept on the same level. Here are considered only observations obtained on February 11th as observations performed on February 10th do not show noticeable changes in (O – C) differences comparable to it precision.

5.1.2. NEA 2021 CA6 (K21C06A)

The NEA 2021 CA6 (K21C06A) was discovered on February 10th, 2021 by Pan-STARRS1 (Haleakala) and had CA to the Earth at 15:58 on February 13th with minimal distance of 0.00111 AU (0.43 lunar distances). The asteroid belongs the Apollo group as previously analyzed one but has much smaller value of MOID with the Earth equals to 0.00037 AU or 0.144 lunar distances. The asteroid was observed during just 3 days with obtained 66 positions in total (22 positions were obtained at Lishan telescope). The observations at Lishan telescope are last ones in current apparition and they are only ones performed after CA time moment. Comparison of the obtained positions with JPL's HORIZONS ephemeris system showed big residuals which significantly decreased when this data was added to the MPC database. Table 8 lists values of the (O – C) differences for the positions obtained from observations at Lishan telescope on February 13th which were calculated before (1) and after (2) consideration these positions in orbit calculations.

Initial calculations show residual equal − 2.03 ″ in right ascension which might seem as wrong identification of the object or any measuring errors. However, the precision is good enough (SD equals to 0.25 ″) and recalculation of the orbit shows significant decreasing of mean value (to − 0.03 ″) which indicates the initial orbit were determined with low accuracy.

5.2. Preliminary orbit improvement

The orbit determination and calculations of ephemerides with future position were done by Find_Orb software of Project Pluto[12] with using current JPL Planetary and Lunar Ephemerides DE440/441 (Park et al., 2021). Obtained data for newly discovered NEAs were used in combination with available positions from MPC database to analyze an improvement of the orbit determination and evaluate the accuracy of predicted positions in the next CA to the Earth. The data according future CA time moments was taken from CNEOS with minimum distance to the Earth less than 0.2 *AU* as a selection criterion. The precision of determined orbital elements are listed in Table 9 for selected newly discovered NEAs observed on the Lishan (O85) and KT-50 (089) telescopes. The two cases of calculations were done for each specified object: 1) observations excluding ±0.5 day on the moment of minimum distance to the Earth in current CA were considered; 2) all available observations were applied in order to calculate the orbit and ephemerid in next CA. Last 2 columns in Table 9 show the date of the closest future CA inside of selection criterion and mean uncertainty of predicted positions on that date. The CA event was chosen here due to the fact that object's apparent brightness is higher during this time thus the observability of the object increases.

It is seen, that adding new positions to computation of the orbital elements in most cases improves its precision and reduces sky uncertainty of ephemerid positions on a future date. Even if time moment of minimum distance to the Earth is inside of observed orbital arc these data could significantly affect the calculations and changes computed orbits of newly discovered NEAs. Among considered NEAs, the CA time moment was at the end of observed orbital arc for K20C01X, K20S00W and

[12] Find_Orb: Orbit determination from observations, https://www.projectpluto.com/find_orb.htm.

Table 9
The precision of computed orbital elements and sky uncertainty of predicted positions for selected newly discovered NEAs.

NEA		N	rms	a	e	i	n	Ω	ω	MA	CA	σ
		obs	(″)	(*AU*)		(*deg*)	(*deg day*$^{-1}$)	(*deg*)	(*deg*)	(*deg*)		(″)
K20C01X	all	170	0.47	7.5E-09	3.7E-07	2.6E-05	1.1E-08	3.8E-06	3.1E-05	1.2E-05	2022-02-18	0.108
	w/o CA	159	0.48	8.0E-09	3.9E-07	2.8E-05	1.2E-08	4.2E-06	3.2E-05	1.3E-05		0.115
K20G02D	all	427	0.35	1.0E-05	1.7E-06	3.9E-05	1.7E-06	4.1E-06	1.0E-05	1.3E-04	2031-04-14	1136
	w/o CA	398	0.33	1.0E-05	1.7E-06	3.8E-05	1.7E-06	4.0E-06	1.0E-05	1.3E-04		1151
K20M03X	all	153	0.32	3.8E-05	3.3E-05	9.0E-04	3.8E-05	1.1E-04	1.2E-03	8.0E-03	2025-11-27	1698
	w/o CA	129	0.32	3.9E-05	3.4E-05	1.0E-03	3.9E-05	1.2E-04	1.3E-03	9.0E-03		1781
K20N01K	all	120	0.29	1.2E-03	2.8E-04	1.9E-02	7.8E-04	1.5E-03	2.5E-02	5.7E-02	2043-08-04	173d
	w/o CA	109	0.27	1.3E-03	3.1E-04	2.1E-02	8.4E-04	1.6E-03	2.7E-02	6.0E-02		172d
K20R00J	all	120	0.56	4.4E-04	1.4E-04	2.6E-03	1.5E-04	6.0E-05	7.0E-04	1.6E-02	2161-08-06	116d
	w/o CA	86	0.42	6.4E-04	2.1E-04	3.8E-03	2.2E-04	7.0E-05	1.0E-03	2.3E-02		129d
K20S00W	all	219	0.43	3.9E-06	6.0E-06	4.5E-04	6.7E-06	9.0E-05	1.3E-03	1.6E-03	2030-03-29	400
	w/o CA	87	0.36	1.4E-05	1.8E-05	1.6E-03	2.3E-05	3.7E-04	4.8E-03	5.2E-03		1359
K20W05U	all	277	0.3	1.9E-08	2.9E-08	1.5E-05	2.4E-08	1.5E-06	1.4E-05	1.3E-05	2033-01-11	0.350
	w/o CA	242	0.23	1.9E-08	3.0E-08	1.5E-05	2.5E-08	1.7E-06	1.4E-05	1.3E-05		0.377
K21C06A	all	49	0.69	2.6E-05	3.5E-05	1.3E-03	3.1E-05	4.0E-05	4.7E-04	4.7E-03	2022-08-11	222
	w/o CA	27	0.55	3.9E-05	5.1E-05	2.0E-03	4.7E-05	1.1E-04	1.5E-03	7.0E-03		333
K21J01G	all	178	0.35	3.3E-05	3.0E-05	1.7E-04	3.1E-05	1.4E-04	3.4E-04	1.3E-03	2034-11-07	1857
	w/o CA	136	0.36	9.9E-05	8.9E-05	5.0E-04	9.3E-05	5.2E-04	1.1E-03	4.1E-03		5893
K21M01E	all	114	0.43	4.3E-05	3.3E-05	2.5E-03	4.7E-05	5.4E-05	5.0E-03	6.0E-03	2027-06-23	1717
	w/o CA	96	0.41	5.6E-05	4.3E-05	3.3E-03	6.2E-05	7.0E-05	6.0E-03	8.0E-03		2576
K21M01K	all	305	0.39	4.4E-08	1.0E-07	2.5E-05	1.1E-07	4.3E-06	1.2E-05	2.4E-05	2029-07-02	0.803
	w/o CA	286	0.36	4.4E-08	1.0E-07	2.5E-05	1.1E-07	4.4E-06	1.2E-05	2.4E-05		0.713
K21N04M	all	69	0.49	7.9E-05	5.1E-05	2.9E-03	7.1E-05	3.7E-05	4.6E-03	6.0E-03	2048-07-13	26d
	w/o CA	41	0.39	9.1E-05	5.9E-05	3.3E-03	8.2E-05	4.2E-05	5.4E-03	7.0E-03		389′
K21U09M	all	200	0.41	8.0E-04	1.4E-04	4.8E-04	1.4E-04	2.8E-04	6.0E-04	4.6E-03	2029-02-08	406′
	w/o CA	179	0.42	1.0E-03	1.8E-04	6.0E-04	1.8E-04	3.6E-04	7.0E-04	5.8E-03		547′

K21C06A. It is also noticeable that the accuracy of predicted positions depends on time span to the next date of CA. In the same time, for three NEAs (K20C01X, K20W05U and K21M01K) which have long observation histories and well-defined orbits (see the uncertainty parameter in Table 4) the accuracy of predicted ephemerides is high enough (less than 1 arcsec) and improvement is minimal. However, the most considered cases have the accuracy of predicted positions which significantly exceeds the FOV of short-focus telescopes and observational campaign will require bigger area of searching. Therefore, it indicates that such objects might be lost in the future and additional observations are substantial. Using the RDS CCD technique eliminates the influence of high apparent rate of motion. It is important for observations of the objects from second group described in Section 2 (last observation was taken before time moment of minimum distance to the Earth) which increases the number of obtained positions and extends the observation arc, resulting in an increase in the accuracy of the determined orbit.

6. Conclusions

The goal of current research project is obtaining high precision astrometric positions of newly discovered NEAs and PHA during their discovery apparition. These objects generally have small amount of observations and, that particularly important, short observation history which result in poorly determined orbits and high positional uncertainties. Additional observations even within one day during time moment of minimal distance to the Earth could significantly change determined orbit and increase its accuracy. The increasing apparent brightness at this time improves observability of these objects however increasing of apparent rate of motion imposes restrictions on the exposure time. As shown in presented paper, used RDS CCD technique implemented on two small-aperture telescopes allows to eliminate high apparent rate of motion affects during observations and achieve sufficient positional precision.

The astrometric results currently obtained and described in the paper show average precision around 0.2″ in both coordinates with respect to JPL's HORIZONS ephemeris system as reference. The performed analysis shows the achieved precision is sufficient and comparable to results of other observatories staying at the same level for newly discovered fast-moving NEAs. Additional analysis of obtained positions regarding to positional precision in along-/cross-track projections does not indicate any significant systematic errors which excludes timing inaccuracy or measurement errors.

Observations obtained in current project in cases of newly discovered NEAs K21C00O, K21C06A extend observed orbital arc which effect in notable orbit improvement. As well as the analysis of available data for such objects shows general influence of observations during the day of minimum distance to the Earth on orbit determination.

Declaration of competing interest

The authors declare that they have no known competing financial interests or personal relationships that could have appeared to influence the work reported in this paper.

Acknowledgement

This research is supported by National Natural Science Foundation of China (Grant No.12073062), the Shanghai Observatory's key cultivation project (N20210601003), Civil Aerospace ”14th Five-Year” Technology Pre-research Project (KJSP2020020203), the Preresearch Project on Civil Aerospace Technologies funded by China National Space Administration (Grant No. D010105) and National Astronomical Data Center of China.

References

Astropy Collaboration, et al., 2013. Astropy: a community python package for astronomy. A&A 558, 33. https://doi.org/10.1051/0004-6361/201322068.
Boattini, A., D'Abramo, G., Valsecchi, G.B., Carusi, A., 2007. A new protocol for the astrometric follow-up of near-earth asteroids. EM&P 100, 31. https://doi.org/10.1007/s11038-006-9075-9.
Boattini, A., Forti, G., 2000. The recovery of near-earth asteroids. P&SS 48, 939. https://doi.org/10.1016/S0032-0633(00)00060-X.
Bowell, E., Koehn, B.W., Wasserman, L.H., Muinonen, K., 1997. Hierarchical observing protocol (hop) for asteroids. DPS 29, 974.
Gaia Collaboration, et al., 2016. The gaia mission. A&A 595, A1. https://doi.org/10.1051/0004-6361/201629272.

Gaia Collaboration, et al., 2018. Gaia data release 2. summary of the contents and survey properties. A&A 616, A1. https://doi.org/10.1051/0004-6361/201833051.

Harris, A.W., Chodas, P.W., 2021. The population of near-earth asteroids revisited and updated. Icarus 365, 114452. https://doi.org/10.1016/j.icarus.2021.114452.

Harris, C.R., Millman, K.J., van der Walt, S.J., Gommers, R., Virtanen, P., Cournapeau, D., Wieser, E., Taylor, J., Berg, S., Smith, N.J., Kern, R., Picus, M., Hoyer, S., van Kerkwijk, M.H., Brett, M., Haldane, A., Fernandez del Rio, J., Wiebe, M., Peterson, P., Gerard-Marchant, P., Sheppard, K., Reddy, T., Weckesser, W., Abbasi, H., Gohlke, C., Oliphant, T.E., 2020. Array programming with NumPy. Nature 585, 357. https://doi.org/10.1038/s41586-020-2649-2.

Heinze, A.N., Denneau, L., Tonry, J.L., Smartt, S.J., Erasmus, N., Fitzsimmons, A., Robinson, J.E., Weiland, H., Flewelling, H., Stalder, B., Rest, A., Young, D.R., 2021. Neo population, velocity bias, and impact risk from an atlas analysis. Planet Sci.J 2, 12. https://doi.org/10.3847/PSJ/abd325.

Jenness, T., Berry, D.S., 2013. Pal: a positional astronomy library. In: Friedel, D.N. (Ed.), Astron.Data.Ann.Software.Syst XXII, 307.

Maigurova, N.V., Pomazan, A.V., Shulga, A.V., 2018. High-precision follow-up observations of near-earth objects. Odessa Astronomical Publications 30, 216. https://doi.org/10.18524/1810-4215.2018.31.144562.

Marsden, B.G., Williams, G.V., 1998. The neo confirmation page. P&SS 46, 299. https://doi.org/10.1016/S0032-0633(96)00153-5.

Park, R.S., Folkner, W.F., Williams, J.G., Boggs, D.H., 2021. The jpl planetary and lunar ephemerides de440 and de441. AJ 161, 105. https://doi.org/10.3847/1538-3881/abd414.

Perna, D., Barucci, M.A., Fulchignoni, M., 2013. The near-earth objects and their potential threat to our planet. A&ARev 21, 65. https://doi.org/10.1007/s00159-013-0065-4.

Pomazan, A., Tang, Z.H., Maigurova, N., Tang, K., Yu, Y., Mao, Y.D., 2021. The research objectives and observational possibilities for fast moving near-earth asteroids. RAA 21, 175. https://doi.org/10.1088/1674-4527/21/7/175.

Roa, J., Farnocchia, D., Chodas, P.W., Chesley, S.R., Park, R.S., Naidu, S.P., 2020. Recoverability of known near-earth asteroids. AJ 160, 250. https://doi.org/10.3847/1538-3881/abbad0.

Tang, Z.H., Mao, Y.D., Li, Y., Yu, Y., Shulga, O., Kozyryev, Y., Sybiryakova, Y., 2014. Precise astrometry of near-earth-object with rotating-drift-scan ccd. Memor. Soc. Astronom. Ital. 85, 821. URL: https://ui.adsabs.harvard.edu/abs/2014MmSAI..85..821Z/abstract.

Vaduvescu, O., Hudin, L., Mocnik, T., Char, F., Sonka, A., Tudor, V., Ordonez-Etxeberria, I., Diaz Alfaro, M., Ashley, R., Errmann, R., Short, P., Moloceniuc, A., Cornea, R., Inceu, V., Zavoianu, D., Popescu, M., Curelaru, L., Mihalea, S., Stoian, A.M., Boldea, A., Toma, R., Fields, L., Grigore, V., Stoev, H., Lopez-Martinez, F., Humphries, N., Sowicka, P., Ramanjooloo, Y., Manilla-Robles, A., Riddick, F.C., Jimenez-Lujan, F., Mendez, J., Aceituno, F., Sota, A., Jones, D., Hidalgo, S., Murabito, S., Oteo, I., Bongiovanni, A., Zamora, O., Pyrzas, S., Genova-Santos, R., Font, J., Bereciartua, A., Perez-Fournon, I., Martinez-Vazquez, C.E., Monelli, M., Cicuendez, L., Monteagudo, L., Agulli, I., Bouy, H., Huelamo, N., Monguio, M., Gansicke, B.T., Steeghs, D., Gentile-Fusillo, N.P., Hollands, M.A., Toloza, O., Manser, C.J., Dhillon, V., Sahman, D., Fitzsimmons, A., McNeill, A., Thompson, A., Tabor, M., Murphy, D.N.A., Davies, J., Snodgrass, C., Triaud, A.H.M.J., Groot, P.J., Macfarlane, S., Peletier, R., Sen, S., Ikiz, T., Hoekstra, H., Herbonnet, R., Kohlinger, F., Greimel, R., Afonso, A., Parker, Q.A., Kong, A.K.H., Bassa, C., Pleunis, Z., 2018. 280 one-opposition near-earth asteroids recovered by the euronear with the isaac Newton telescope. A&A 609, 105. https://doi.org/10.1051/0004-6361/201731844.

Veres, P., Farnocchia, D., Chesley, S.R., Chamberlin, A.B., 2012. Improved asteroid astrometry and photometry with trail fitting. PASP 124, 1197. https://doi.org/10.1086/668616.

Veres, P., Jedicke, R., Denneau, L., Wainscoat, R., Holman, M.J., Lin, H.W., 2017. Statistical analysis of astrometric errors for the most productive asteroid surveys. Icarus 296, 139. https://doi.org/10.1016/j.icarus.2017.05.021.

Veres, P., Payne, J., Holman, M.J., Farnocchia, D., Williams, G.V., Keys, S., Boardman, I., 2018. Unconfirmed near-earth objects. AJ 156 (5). https://doi.org/10.3847/1538-3881/aac37d.

Virtanen, P., Gommers, R., Oliphant, T.E., Haberland, M., Reddy, T., Cournapeau, D., Burovski, E., Peterson, P., Weckesser, W., Bright, J., van der Walt, S.J., Brett, M., Wilson, J., Millman, K.J., Mayorov, N., Nelson, A.R.J., Jones, E., Kern, R., Larson, E., Carey, C.J., Polat, İ., Feng, Y., Moore, E.W., VanderPlas, J., Laxalde, D., Perktold, J., Cimrman, R., Henriksen, I., Quintero, E.A., Harris, C.R., Archibald, A.M., Ribeiro, A.H., Pedregosa, F., van Mulbregt, P., SciPy 1.0 Contributors, 2020. Scipy 1.0: fundamental algorithms for scientific computing in python. Nat. Methods 17, 261. doi:10.1038/s41592-019-0686-2.

Xie, R., Bennett, N.J., Dempster, A.G., 2021. Target evaluation for near earth asteroid long-term mining missions. Acta Astronom. 181, 249. https://doi.org/10.1016/j.actaastro.2021.01.011.

Yu, Y., Zhao, X.F., Luo, H., Mao, Y.D., Tang, Z.H., 2018. Application of ccd drift-scan photoelectric technique on monitoring geo satellites. Adv. Space Res. 61, 2320. https://doi.org/10.1016/j.asr.2018.02.005.